Sādhanā (2023) 48:188
https://doi.org/10.1007/s12046-023-02243-8

Synthesis and characteristics evaluation of magnesium alloy (AZ91) nanocomposite developed with ZrO_2 via liquid state stir cast process

R KARTHIK[1,*], N SHIVA SANKARAN[2], K VENKATESH RAJA[3] and R VENKATESH[4]

[1]Department of Mechanical Engineering, Kongunadu College of Engineering and Technology, Tholurpatti, Tamil Nadu 621215, India
[2]Department of Mechanical Engineering, Selvam College of Technology, Namakkal, Tamil Nadu 637003, India
[3]Department of Mechanical Engineering, Sona College of Technology, Salem, Tamil Nadu 636005, India
[4]Department of Mechanical Engineering, Saveetha School of Engineering, SIMATS, Chennai, Tamil Nadu 602105, India
e-mail: karthikramasundaram@gmail.com; shivasankaran.n@gmail.com; kvenkateshraja@hotmail.com; venkidsec@gmail.com

MS received 3 March 2023; revised 6 June 2023; accepted 12 June 2023

Abstract. With a high strength-to-weight ratio, the AZ91 grade magnesium alloy is essential in various engineering applications like automotive, aerospace, marine, and defence. The main drawback of magnesium casting has oxidation results in agglomeration, slag formation, and voids. The present investigation of the liquid state vacuum stir cast process under an inert atmosphere was utilized to prepare AZ91 alloy nanocomposites with 0, 3, 6, 9, and 12 wt% of nano-zirconium dioxide (ZrO_2) particles. The microstructure elemental composition of the developed composites was subjected to SEM/EDS analysis. The effect of ZrO_2 nanoparticles on the composite's physical, mechanical, wear, and corrosion properties was studied. The composite's actual density obeys the mixture's rule and is found to be lightweight compared to conventional materials. The composite contained 9 wt% of ZrO_2 and showed the maximum micro Vickers hardness number (96.71 ± 1.05 HV), ultimate tensile (281 ± 1.1 MPa), and impact strength (20.61 J). The higher content of ZrO_2 offered good wear resistance (value) under 40 N at 1 m/sec sliding speed compared to unreinforced cast AZ91 alloy and facilitated higher corrosion resistance of 3.23 mm/year.

Keywords. AZ91; characteristics study; inert atmosphere; vacuum stir cast; ZrO_2.

1. Introduction

Magnesium alloy-based matrix materials were found as potential materials for various industrial applications due to their high strength-to-weight ratio, superior dimensional stability, low density, defect-free castability, good electrical and thermal conductivity, and vibration damping properties and also gathering importance in bio-implant application due to their superior biodegradation and physical affinity for bone tissue compared to some other metallic elements [1, 2]. Moreover, magnesium and its alloy were drawbacks of low corrosion resistance and were not adopted for biodegradable implants [3, 4]. To overcome the demerits, surface treatment like the Pulsed-electro deposition method (PED) was adopted and reported that the corrosion resistance of magnesium alloy (AZ31) was improved [5]. Extrusion [6, 7], and alloying technique [8]. The magnesium alloy combinations like Al/Zn gathered significance in the positive corrosion approach under the NaCl environment [9].

However, poor corrosion behaviour is observed in AZ 91 alloys due to micro galvanic corrosion and Ni, Fe, and Cu metal impurities [10]. In addition, using manufacturing processes such as extrusion, magnesium materials have a fine-grained, relatively uniform micro-structural with improved resistance to corrosion. The combinations of soft matrix and hard reinforcement phases found enhanced mechanical, tribological, and corrosion properties reported by Ghasli *et al* [11] and based on the report by Venkatesh *et al* [12] studied the Characterization of Mechanical Properties of AA8014 + Si_3N_4/ ZrO_2 Hybrid Composites by Stir Casting Process.

Moreover, the interaction of varied preparation techniques, variations in the solidification process, and coatings can influence the microstructural interactions and result in significantly different electrochemical behaviour. In high-strength applications in the automotive and aerospace industries, MMCs are crucial. The work of ZE41A confirms that the ceramic reinforcement increases the alloy's

*For correspondence
Published online: 29 August 2023

mechanical and corrosion behaviour [13]. Also, the homogenous distribution of reinforcements enhances surface properties (tribological properties) [14]. The AZ91 alloy shows a 1.2 mm/year corrosion rate, whereas the corrosion rate of AZ31 is 1.1 mm/year [15]. The Mg metal matrix composites were optimized, and optimal parameters for stir casting and machinability were identified [16, 17]. The demand for magnesium alloy-based lightweight materials was increased progressively in various applications due to light and specific strength compared to traditional materials like aluminium and titanium. In the past decades, ceramic-based (Al_2O_3, B_4C, SiC, TiC, CNT, and ZrO_2) reinforcements were employed in prior studies on AZ91 alloys [18–21].

Among the various reinforcements, zirconium dioxide (ZrO_2) has a high elastic modulus, low friction, and a high melting temperature. Because of these properties, there are numerous instances where ZrO_2 has been used as reinforcement in specimens with magnesium matrixes. So, the work is framed to analyze the effect of nano ZrO_2 on AZ91 alloy. It is known that nanoparticles significantly influence the behaviour of any composites. Obtaining experiments on nanocomposite reinforced with nano ZrO_2 and AZ91 is challenging. According to prior research findings, AZ91 + ZrO_2 composites' mechanical and corrosion behaviour has yet to be thoroughly reviewed.

2. Materials and methods

2.1 *Matrix and reinforcements*

Magnesium alloy AZ91 grade is chosen as the matrix material due to its enhanced mechanical properties, ease of casting, dimensional stability, and good thermal behaviour [22]. The primary constituents of AZ91 alloy are 9.2% of Al, 0.45–0.8% of Zn, 0.17–0.5% of Mn, and 90% of Mg.

The 50 nm-sized zirconium dioxide (ZrO_2) particles were selected as the reinforcement phase. Generally, ZrO_2 particle has high structural stability, hardness, and wear resistance [23]. The AZ91 alloy and ZrO_2 microstructural images are shown in figures 1(a) and 1(b).

2.2 *Fabrication of AZ91 alloy nanocomposites*

The synthesis of AZ91-ZrO_2 nanocomposite is called the liquid state vacuum stir cast process due to its simplicity, ease of operation, ability to produce any complex shape, and economical mass production [24].

The representation of matrix/reinforcement, the actual experimental setup of the vacuum stir casting process, and the developed composite is shown in figure 2. Primarily, five composite specimens were fabricated with and without reinforcements. Constitutions are tabulated in table 1. The nano ZrO_2-reinforced composites were found to improve compressive characteristics, strength, toughness, and density wear resistance [25].

Based on table 1, the matrix and reinforcements are weighted. The AZ91 alloy ingots are placed in a graphite crucible and heated to 850°C under an inert atmosphere. It is significantly greater than the temperature to melt the AZ91 at 650°C, which helps to increase the solubility.

The reinforcement of the ZrO_2 (3, 6, 9, and 12%) was also externally preheated into the muffle furnace at 850°C. Additionally, ZrO_2 is placed in different containers and preheated to 850°C in a furnace. Finally, heated and preheated matrix and reinforcement were added to the 500°C as a semi-solid mould cavity. The molten magnesium material reached after 900°C is taken into account, adding 10g of degasser to remove impurities and prevent oxidation. However, nanoparticle ZrO_2 is preheated before addition.

A mechanical twin-blade stirrer was inserted into the crucible furnace in vertical directions. The mixture is designed to actuate at a speed of 450 rpm. After liquefaction, the mould dies were preheated to 500°C to reduce the possibility of deformation, shrinkage, and blow holes. The unreinforced cast AZ91 alloy and the nanocomposites of the defined composition (table 1) were prepared. The

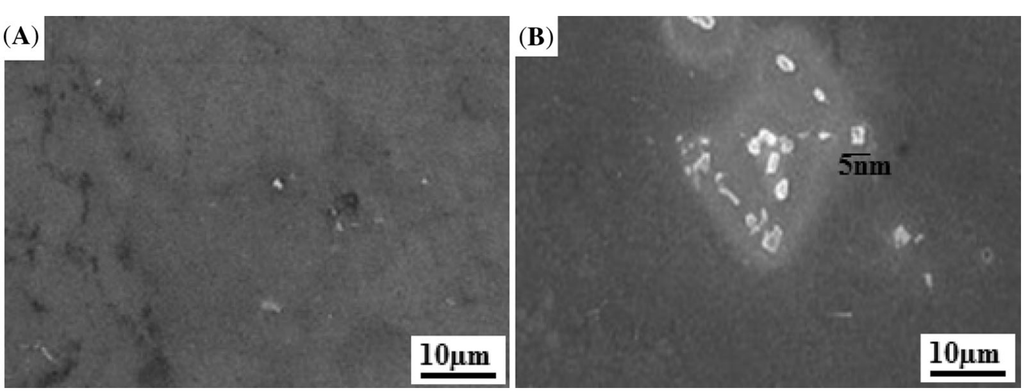

Figure 1. Scanning electron microscope micrograph of a) AZ91 and b) ZrO_2.

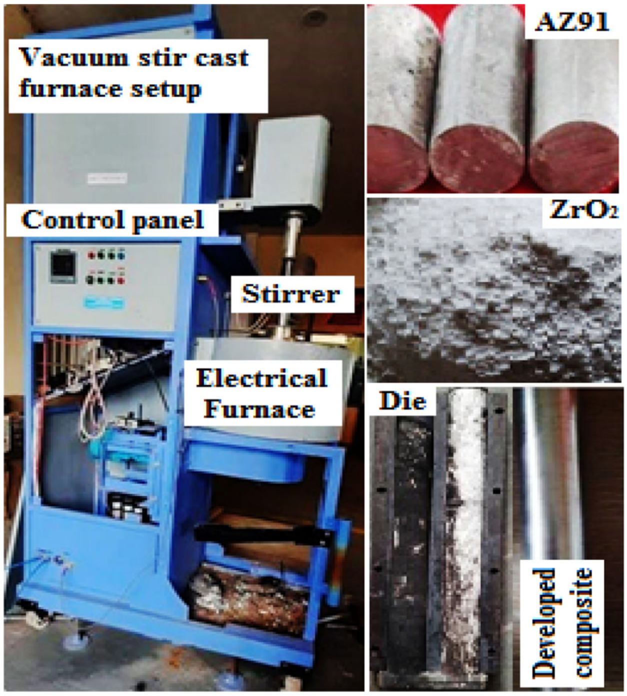

Figure 2. Fabrication of magnesium alloy (AZ91) nanocomposites.

Table 1. Compositions/weight of matrix/reinforcements

	Weight in grams	
Composites	AZ91	ZrO_2
AZ91-as cast	1500	0
AZ91-3% ZrO_2	1455	45
AZ91-6% ZrO_2	1410	90
AZ91-9% ZrO_2	1365	135
AZ91-12% ZrO_2	1320	180

molten magnesium matrix was mixed with reinforcing phase ceramic nanoparticles before being heated to 850°C in a furnace. The furnace was raised to 850°C. After reaching the desired temperature, the continuous stirrer of 450 rpm evenly dispersed the reinforcements within the furnace. The continuous stirring action was maintained for 10 minutes at a constant temperature to ensure the uniform distribution of reinforcement in the AZ91 matrix. Finally, a pressure of 0.1 MPa was applied, and the cast was developed as a cylindrical rod (50 mm diameter), as shown in figure 2.

2.3 *Characterization of developed composites*

2.3.1 *Measurements of density and porosity* Based on the principle of Archimedes and the rule of mixture, composites' actual and theoretical density was measured. Equation 1 and 2 represents the experimental (actual) and theoretical density measurement. The percentage of porosity volume of each specimen was estimated based on Eq. (3).

$$\rho_{Experimental} = \left[\frac{m_{air}}{m_{air-}m_{water}}\right] x\rho_{water} \tag{1}$$

where ρ_{water} the density of water (0.998 g/cm^3 at 20°C) and mass of the specimen were represented in air and water by m_{air} and m_{water}, respectively.

$$\rho_{Theoretical} = \rho_{AZalloy} W_{AZalloy} + \rho_{ZrO_2} W_{ZrO_2} \tag{2}$$

where W and ρ are the weight fraction and density.

$$porosityin\% = \left(1 - \frac{\rho_{Experimental}}{\rho_{Theoretical}}\right) x100 \tag{3}$$

2.3.2 *Measurement of mechanical properties* The developed composites' hardness was evaluated during the 402MVD model micro Vickers Hardness testing Machine followed by ASTM384 standards. The specimens were prepared to get smooth flat sand polished specimens loaded at 300 g for 10 seconds. Three trials from each specimen were tested for average hardness values noted as mean; same trend, tensile behaviour of AZ91 alloy and its composites was performed according to ASTM E8-M09, and its dimension is 100 mm × 10 mm × 6 mm. The Charpy impact machine is used to determine the impact strength of the composite. Tests have been carried out on a specimen with dimensions of 10 mm × 10 mm × 55 mm and 2 mm depth with a V-notch of 45° angles.

2.3.3 *Measurement of wear properties* The wear behaviour of developed AZ91 alloy composite with and without ZrO_2 is studied by hardened steel counterface attached with Ducom pin on disc wear testing machine with an applied load of 10, 20, 30, and 40 N under a 1 m/sec sliding velocity. The ASTM G99 standard follows it.

2.3.4 *Electrochemical corrosion test* The synthesized AZ91 alloy and its composites were prepared by the dimensions of 10 mm × 10 mm × 3 mm were prepared from the cast block. The specimens were blended using various silicon carbide waterproof abrasive sheets and continued to use acetone, and an ultrasonic cleaner. The three-electrode systems like platinum as the cathode, saturated calomel electrode (SCE) as the positive reference electrode, and work material as the anode. The composite's open circuit potential (OCP) has been tested for a minimum of 60 mins or until the stable potential. The sweep orientation was also changed to the complete reverse electrode direction when the current density attained 2 mA/cm^2. Electrochemical impedance spectroscopy (EIS) was carried out on the revealed OCP moral

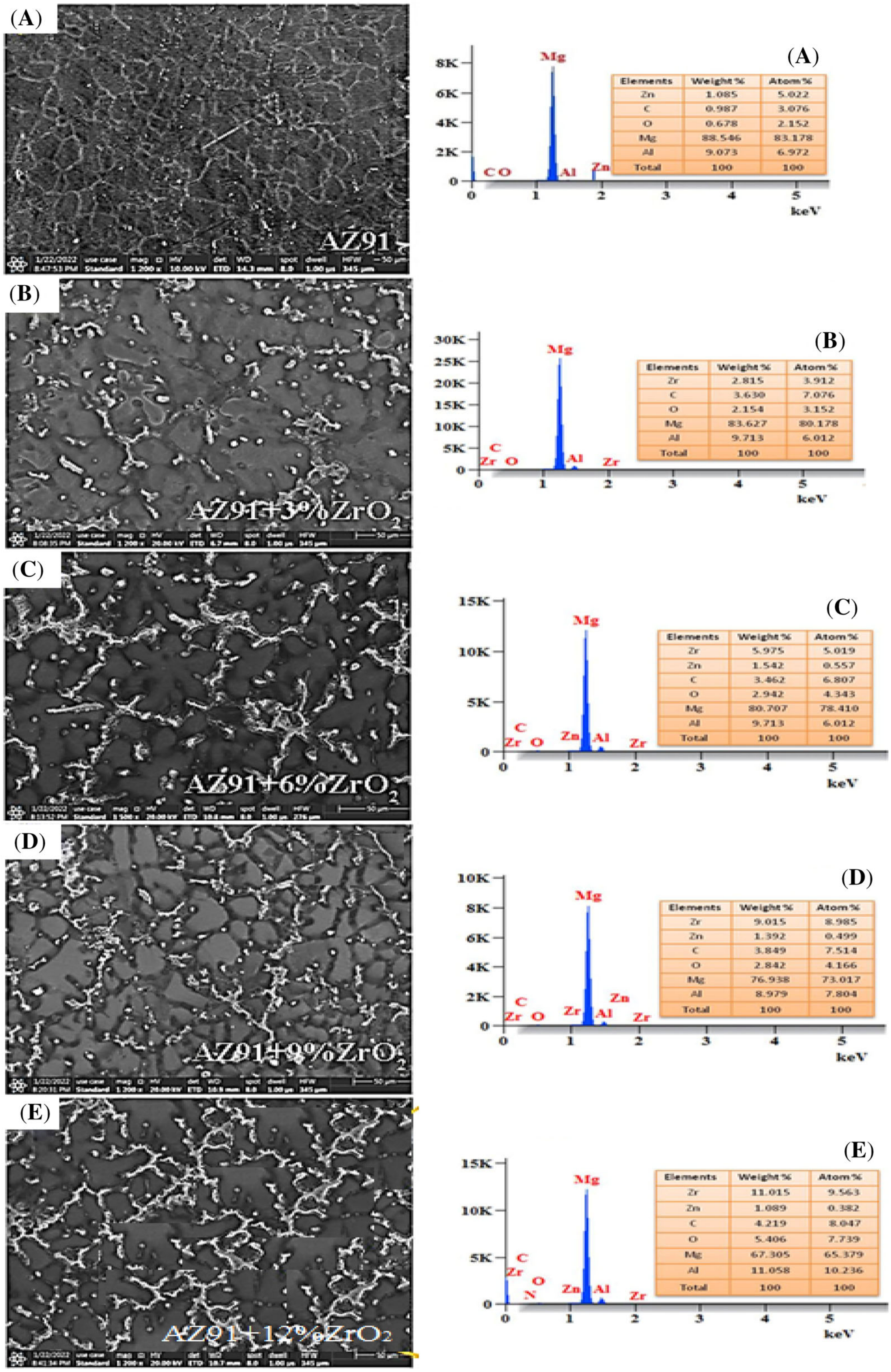

Figure 3. SEM-EDS micrograph and spectrograph of developed composites a) AZ91/0wt% ZrO2, b) AZ91/3wt% ZrO_2, c) AZ91/6wt% ZrO_2, d) AZ91/9wt% ZrO_2, e) AZ91/12wt%. ZrO_2

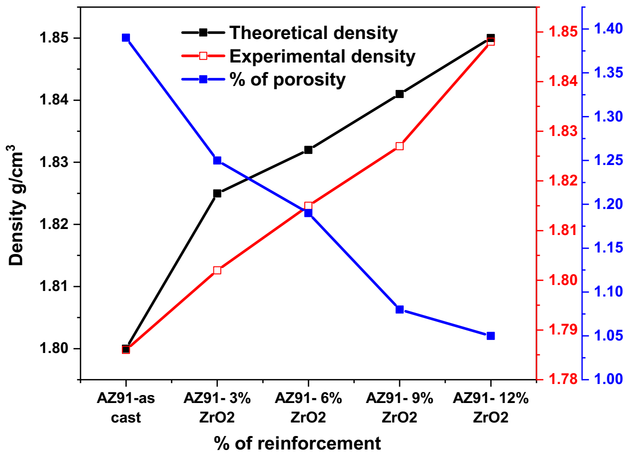

Figure 4. Density and porosity level of developed composites.

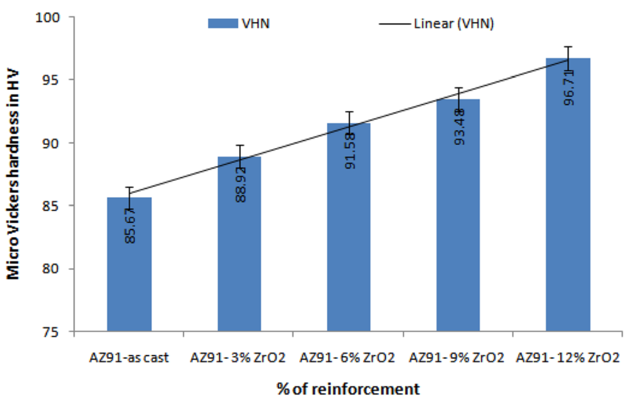

Figure 5. Micro Vickers hardness of developed composite.

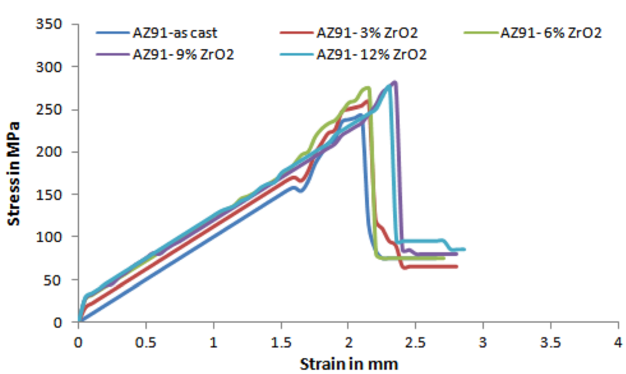

Figure 6. Stress-strain plot for developed composites.

standards using an oscillation of 20 mV in an intensity spectrum of 1×10^{-5} Hz to 1×10^{-2}. Results from individual electrochemical corrosion tests using a Gamry reference 600 tool mechanism were performed in a 3.5%

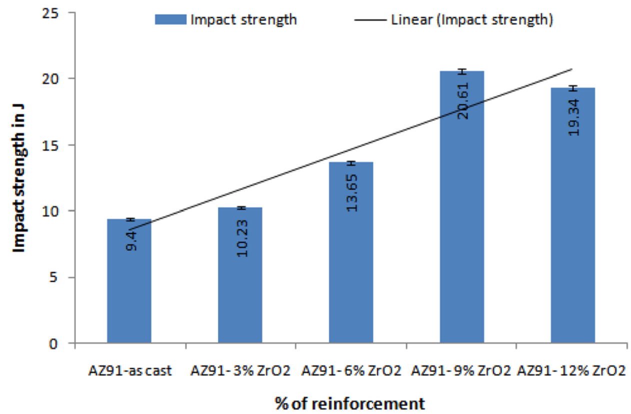

Figure 7. Charpy impact strength of developed composites.

NaCl solution representing extreme possible environmental conditions.

3. Results and discussion

3.1 *Scanning electron microscope with EDS spectrograph*

The scanning electron microscope with EDS images of unreinforced and different weight percentages of ZrO_2 reinforced AZ91 alloy nanocomposite is shown in figure 3(a–e). Figure 3(a) represents that varying the casting technique significantly affects the shape and morphological properties of secondary phase particles in the AZ91 composite.

The detailed EDS illustration shows the various peaks and found Mg is the major peak. Figure 3(b) reveals the uniform distribution of ZrO_2 nanoparticles in the AZ91 matrix and found few slags due to the melting point temperature of AZ91. It was due to improper stir speed. Similarly, the EDS represent the minor peak for oxide formation. The inert atmosphere helps to reduce oxidation during the melting of AZ91. In AZ91/ZrO_2 composite, the appearance of equiaxed grains confirmed that the reinforced ZrO_2 particles contribute to heterogeneous nucleation, which significantly influences the grain structure, as shown in figure 3(c).

The selection of reinforcement, process, and its parameter decided the distribution of reinforcement [26]. It was observed from figure 3(d) that the structure has a homogeneous distribution of ZrO_2 particles, and there is no evidence for agglomeration, which shows the wettability nature between the matrix and reinforcements. It has no agglomeration or reduction of ZrO_2 nanoparticles in the molten metal, which ensures better wettability of the matrix alloy and its reinforcement.

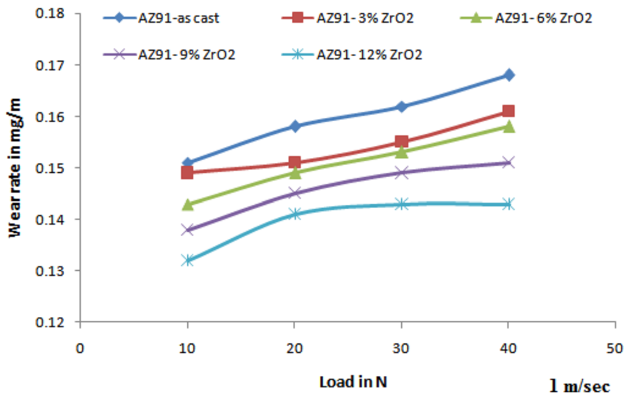

Figure 8. Wear rate of developed composites under 1 m/sec sliding speed.

3.2 *Density and porosity of composites*

Figure 4 shows details of the actual density, theoretical density and porosity of the composites containing 0, 3, 6, 9, and 12 wt% of nano-ZrO_2.

The increase in densities is observed with an increase in the weight percentage of ZrO_2, proving their rule of mixture. AZ91 nanocomposite can be observed as free of casting flaws because the porosity level is less than 5%. But the variations in (actual) experimental and theoretical density may be due to the impurities in raw materials.

It was varied due to casting defects or air entrapment inside the composite [27]. The AZ91 alloy with 12% ZrO_2 has the maximum density (1.84 g/cm^3), higher than the base material. The increase in the reinforcement weight proportion led to an increase in AZ91 alloy matrix composite density. The results of the measured density can clearly show that an increase in the reinforcement ratio raises the density of the metal matrix composites. The 12% ZrO_2 reinforcement of measured experimental density was 3.47% higher than the casted AZ91 alloy and 2.55% higher than 3%ZrO_2 reinforced AZ91 alloy nanocomposites.

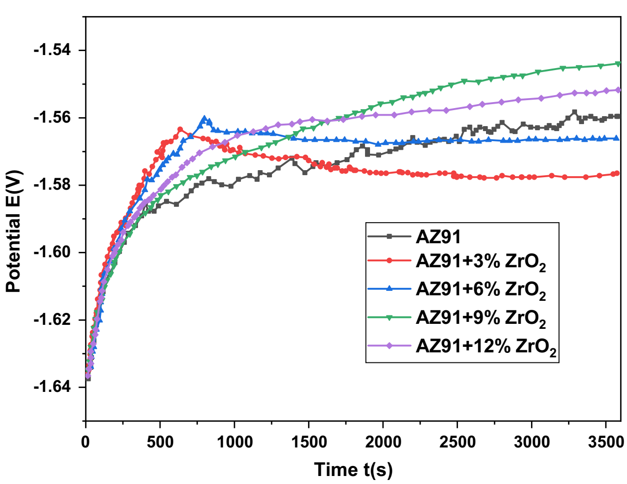

Figure 9. Open circuit potential (OCP) curve of AZ91/ZrO_2 in 3.5% NaCl solution.

3.3 *Micro vickers hardness number of composites*

The micro Vickers hardness of unreinforced and ZrO_2-reinforced AZ91 alloy nanocomposites are shown in figure 5. It showed significant improvement in hardness with increasing reinforcement like 0, 3, 6, 9, and 12 wt%.

The investigational results showed that the hardness of the developed nano ZrO_2-reinforced composites' hardness values consistently converged in a manner that matched the weight percentage of ZrO_2. The hardness of the composite without ZrO_2 nanoparticle was found to be 85.67 $\pm$ 1.1 HV. The additions of nano ZrO_2 in the AZ91 matrix found increased hardness value and met the linear trend line represented by figure 5. Further, the hardness value of the composite is the surface property, and it depends on the material/phase presence on the intended surface; because of this reason, the average hardness value is continuously measured. The maximum hardness of 96.71 $\pm$ 1.05 HV was observed by 12 wt% of ZrO_2 in the AZ91 matrix and increased by 12.88% compared to cast AZ91 alloy without reinforcements. The increase in hardness value depended on the interfacial bond quality of the matrix and reinforcement. The effective and uniform particle distribution with equiaxed grains was the reason for improved hardness, as evidenced in figure 3(e). The hard zirconium dioxide may resist the indentation against the applied load.

3.4 *Stress-strain curve of developed composites*

Figure 6 shows the stress–strain plot for AZ91 alloy composite prepared with 0, 3, 6, 9, and 12 wt% of ZrO_2 nanoparticles. It significantly improves the tensile strength of the composite due to homogenous particle distribution, which strengthens the composite structure and resists particle dislocation. The tensile strength of unreinforced AZ91 alloy cast was found to be 242 $\pm$ 1.2 MPa, and the additions of 3, 6, and 9 wt% of nano ZrO_2 showed the increased tensile strength of 6.6%, 13.2%, and 16.11% respectively. Similarly, the elongation due to high tensile load showed an increased strain rate of 2.85 mm.

The nanoparticles can increase the Orowan strengthening, where the reinforced nano ZrO_2 is strong to resist the dislocation penetration. The effective interface necklace formed structure was evidenced in figure 3(b–e). The higher content of ZrO_2 nanoparticles in the AZ91 matrix decreased the tensile strength of 275 $\pm$ 1.21 MPa. The brittle nature reinforcement phase in the composite specimen causes micro-cracks to spread at the dispersion layer of the reinforcing particles during external loads applied to the composites. The secondary phase fiber material limits particle dislocation during high tensile load [28–30].

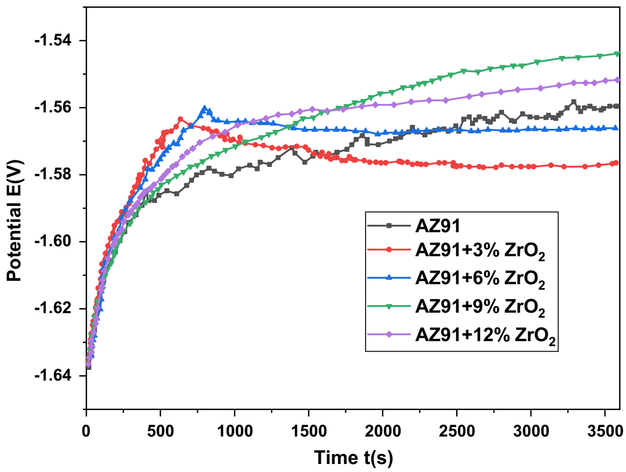

Figure 10. Open circuit potential (OCP) curve of AZ91/ZrO_2 in 3.5% NaCl solution.

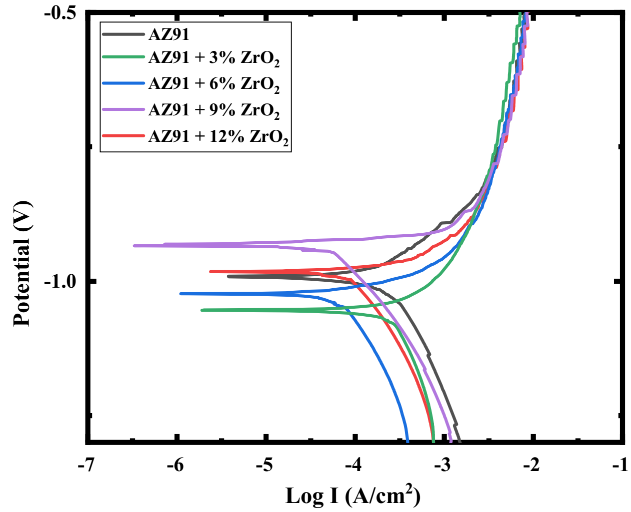

Figure 11. Polarization Curvesof the test specimens.

The clustering and agglomeration of nano-reinforced particles significantly influence the mechanical strength of manufactured composite materials. Both homogeneous dispersions of ZrO_2 particles and interfacial bonding of particles with variable proportions, including matrix material, are the factors that contributed to the combination of high tensile strength.

3.5 *Impact strength of developed composites*

The Charpy impact test was used to assess the impact strength of cast AZ91 alloy and reinforced with different weight percentages of ZrO_2 nanoparticles, as shown in figure 7. The maximum impact strength was 20.61 ± 0.13 J, founded on 9 wt% of reinforcement, and more than 9 wt% ZrO_2 showed decreased impact strength of 19.34 ± 0.31 J. A similar trend in the tensile property of the composite, the impact strength of the composite also improved up to 9 wt% of reinforcement, and after that, it decreased. It was due to the uniform distribution of reinforcement dramatically increasing the impact strength of the composites, and its SEM is evidenced in figure 3(b–d). It is because the agglomeration of particles decreases the impact strength of the composite and leads to localized region failure of the composite.

3.6 *Wear resistance of developed composites*

Figure 8 illustrates the wear rate of AZ91 alloy composite containing different weight percentages of ZrO_2 nanoparticle and incorporation of hard ceramic reinforcement in soft matrix found good wear resistance, which is higher than the wear resistance of cast AZ91 alloy.

The increased wear rate was due to the hardness of the composite's high scratch resistance. Moreover, the composite's wear rate gradually increased with an applied load. A maximum wear resistance of 0.168 mg/m was found on cast AZ91 alloy without reinforcement at 40 N under 1 m/sec sliding velocity. Moreover, the temperature may rise due to high friction between the pin and disc, resulting in adhesive failure. The hard ceramic B_4C in aluminium alloy composite limits the wear rate and increases thermal stability [31].

However, the wear resistance of the composite specimen containing 12 wt% of ZrO_2 facilitates a minimum wear rate of 0.143 mg/m at 40 N load under 12.91 N frictional force. The high friction force may lead to an increased temperature between the pin and disc; it leads to the diffusion of hard ceramic reinforcement in the soft AZ91 matrix as an effective and good interface.

Table 2. Corrosion properties of the AZ91-ZrO_2 composites

Composites	OCP (V)	E_{corr} (V)	I_{corr} (mA/cm^2)	mm/year
AZ91-as cast	−0.9300	−0.9329	0.9783	13.33
AZ91-3% ZrO_2	−1.1232	−1.0584	0.4651	9.99
AZ91-6% ZrO_2	−1.0142	−1.0253	0.3624	7.74
AZ91-9% ZrO_2	−0.9957	−0.9923	0.1521	3.23
AZ91-12% ZrO_2	−0.9925	−0.9913	0.1836	3.87

3.7 *Electrochemical corrosion measurement of developed composites*

Figure 9 shows the OCP curve of cast AZ91 Mg alloy and ZrO_2-reinforced AZ91. The potential (V) of the test specimens was recorded for 3600 seconds in a 3.5% NaCl solution. A dilute NaCl solution was used to analyze of corrosion behaviour of AZ91 alloy [32].

The OCP of AZ91 + 3% ZrO_2 shows significant potential drops due to the initiation of localized corrosion compared with the OCP of cast AZ91 alloy. Because of the potential depletion, there is the possibility of initiation of the magnesium hydroxide film, which involves several cycles of dissolution processes. Recently, the corrosion behaviour of CeO_2 coating magnesium alloy was studied by different electrolytic mediums [33]. The hard ceramic particle may withstand the high thrust force and give the lubricant effect [34].

The potential drop in OCP can be caused by different parameters like pH and temperature (evaluation of hydrogen due to anode and electrolyte interaction). In addition, the potential variation is primarily caused by the dissolution of the passive layer. The process can be applied to a metal surface, demonstrated by the reduction layer from its maximum priority (passive region) to its original value (active region). The OCP of AZ91 + 9% ZrO_2 shifts towards superior predicted values with no observable potential drops during submersion, demonstrating that the protective layer installed in AZ91 is very supportive and firmly applied to the surface. Equation 1 represents the formula to calculate the corrosion rate of the composites [35].

$$Corrosion\,Rate\left(\frac{mm}{year}\right) = \frac{0.00327 \times Eq.wt. \times I_{Corr}}{\rho} \quad (4)$$

where,

Eq. wt. denotes the equivalent weight at the valance of +2(g);

ρ is the density (g/cm^3) and

I_{Corr} denotes the corrosion current density (µA/cm^2).

Electrochemical measurements of corrosion current density can assess the corrosion performance of metallic materials (I_{Corr}) and corrosion potential (E_{Corr}). The dynamic polarization test results for both base material and MMCs immersed in an aqueous solution as shown in figure 10.

The anodic section of the AZ91 specimen exhibits sustained electrochemically active solubility until the density achieves 2 mA/cm^2, at which point the potential is reversed. It indicates that the AZ91 alloy has no passivity. The E_{Corr} of the specimens shows a similar trend as of OCP curve, which states work reported the stable OCP value and the anodic and cathodic nature of the samples are defined based on the OCP value. With the help of the hysteresis, the curve shows that the pitting and corrosive potential are located in the same regions [36]. Therefore, it is desirable to have high E_{Corr} and low $I_{Corr}$for suitable corrosion-resistance composites. Table 2 shows the experimental result of the polarization test E_{corr}(V), I_{corr}(mA/cm^2), and rate of corrosion (mm/year). The corrosion current is the direct indicator of corrosion resistance higher the current, the lower the resistance [37]. The results revealed that the corrosion of the composite increases up to 9% of ZrO_2 reinforcement, and after that, it starts to increase. It may be because of increased localized corrosion due to the agglomeration of reinforcement [38, 39].

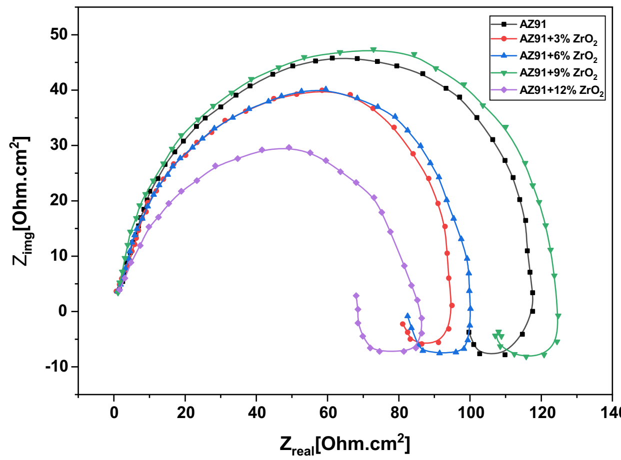

Figure 12. Nyquist plot of AZ91/ZrO_2 in 3.5% of NaCl solution.

Figure 11 shows the polarization curve for tested composite specimens. As already discussed, an electrochemical reaction caused by hydrogen evolution causes magnesium and its alloys to erode in an aqueous solution. The electrochemical reaction between water and matrix composite materials causes them to corrode in aqueous environments, producing magnesium hydroxide and hydrogen gas. Due to the production of OH, the pH rises, which facilitates the chemical reactions that form the Mg hydroxide film. The corrosive environment film modified by MgO and Mg (OH)2 appears to have very poor electrochemical performance, and the presence of accelerated corrosion active surfaces, such as noble coagulates or other electronic impurity states in the composite, significantly accelerates the corrosion rate.

$$\text{Anodic reaction}: \ \mathrm{Mg(s)} = \mathrm{Mg}^{2+}_{(aq)} + 2e^-$$

$$Cathodic\,reaction\, 2H_2O + 2e- = H_2 + 2OH^-$$

$$Mg^{2+}_{(aq)} + 2OH^-_{(aq)} = Mg(OH)_{2(s)}$$

The mixture of NaCl was selected to increase the corrosion rate of the prepared composites, as shown in figure 12. Corrosion of base material at various concentrations was rapidly decreased by the development of surface films on the material. The configuration of the intermetallic compounds film may have caused the OCP of both alloy elements to become high potential at the earlier stages of immersion due to the corrosion protection of the film, which may have acted as a protective barrier to additional oxidation reaction. According to figure 4, the oxide layer film does not entirely protect the surface of the oxide layer film of AZ91, which appears to be compact.

Potentiodynamic anodic polarization techniques evaluated the anti-corrosion behaviour of AZ91 alloys and their composites. EIS carried out the prepared specimens of performance in corrosion resistance conformity experiments. The results of the EIS Impedance response of AZ91/ZrO_2 in 3.5% of NaCl (Nyquist plot) are shown in figure 12. The capacitive loop in the Nyquist plane in magnitude represents the polarisation impedance of the test specimens. A lower corrosion rate is generally associated with a higher polarization resistance. The plot of figure 12 (Nyquist) demonstrates that the two metals have distinct capacitance circuits over the entire frequency range, indicating that the corrosion rate varies despite using the same technique. The corrosion rate of AZ91 + 9%ZrO_2 is significantly greater than that of the unreinforced Mg. Compared to AZ91 magnesium alloy and other reinforcements, AZ91 has a relatively high impedance value, suggesting that AZ91 + 9%ZrO_2 has improved corrosion protection properties.

4. Conclusion

The study demonstrates the effect of nano ZrO_2 (3, 6, 9 and 12 wt%) reinforcement on AZ91 magnesium alloy by analyzing its Microstructural, mechanical, wear, and electrochemical properties. Based on the experimental results, the forthcoming conclusion is derived. The SEM micrograph indicated that ZrO_2 reinforcement dispersed uniformly in the Mg matrix up to 9%. Further increase in reinforcement percentage leads to agglomeration. The optimum results for the reinforcement of 9 wt% ZrO_2 in AZ91 Mg alloy show better mechanical properties with optimum microhardness, tensile, and impact strength improved by 12.9%, 16.11%, and 2.19 times compared to cast AZ91 alloy. Furthermore, the presence of ZrO_2 enables the Orowan strengthening effect, strengthening the composite by restricting dislocation movement. Similarly, the homogeneous distribution of reinforcement limits the crack propagation process, increasing the impact strength of the composite. Like mechanical properties, the corrosion resistance of the AZ91 + 9% ZrO_2 shows a comparatively better corrosion rate of 3.23 mm/year. Similarly, the wear resistance of the developed composite containing 12 wt% of ZrO_2 nanoparticles noted high wear, with a wear resistance of 0.143 Mg/m.

Author contributions All authors contributed to the study's conception and design. Material preparation, data collection and analysis were performed by [R.K], [N.S], [K.V], and [R.V]. The first draft of the manuscript was written by [R.K], and all authors provided language help, writing assistance and proofreading of the manuscript. All authors read and approved the final manuscript.

Funding The authors did not receive support from any organization for the submitted work. No funding was received to assist with the preparation of this manuscript. No funding was received for conducting this study. No funds, grants, or other support were received.

Data availability All the data required are available within the manuscript.

Declarations

Conflict of interest The authors have no competing interests to declare relevant to this article's content.

Ethics approval This is an observational study. Synthesis and characteristics evaluation of magnesium alloy (AZ91) nanocomposite developed with ZrO2 via liquid state stir cast process, Research Ethics Committee has confirmed that no ethical approval is required.

References

[1] Kirkland N T, Lespagnol J, Birbilis N and Staiger M P 2010 A survey of bio-corrosion rates of magnesium alloys. *Corr. Sci.* 52: 287–291

[2] Boby Arun, Pillai U T S and Pai B C 2011 Developments in Magnesium Alloys for Transport Applications—An Overview. *Ind. Foundry J.* 57: 29–37

[3] Qiu Xun, Wan Peng, Tan LiLi, Fan Xin Min and Yang Ke 2014 Preliminary research on a novel bioactive silicon doped calcium phosphate coating on AZ31 magnesium alloy via electrodeposition. *Mat. Sci. Eng: C.* **36** 65–76

[4] Zijian Li, Xunan Gu, Lou Siquan and Zheng Yufeng 2008 The development of binary Mg–Ca alloys for use as biodegradable materials within bone. *Biomaterials* 29: 1329–1344

[5] Sekaran R P, Ramakrishnan H, Venkatesh R and Nithya A 2023 Mechanical and Physical Characterization Studies of Nano Ceramic Reinforced Al–Mg Hybrid Nanocomposites. *Silicon*. https://doi.org/10.1007/s12633-023-02473-9

[6] Przondziono J, Walke W, Hadasik E, Szala J and Wieczorek J 2013 Corrosion resistance tests of magnesium alloy WE43 after extrusion. *Metalurgija.* 52: 243–246

[7] Carboneras M, Peréz-Maceda B T, Del Valle J A, García-Alonso M C, Lozano R M and Escudero M L 2011 In vitro performance of magnesium processed by different routes for bone regeneration application. *Mat. Lett.* 65: 3020–3023

[8] Zijian Li, Xunan Gu, Lou Siquan and Zheng Yufeng 2008 The development of binary Mg-Ca alloys for use as biodegradable materials within bone. *Biomaterials* 29: 1329–1344

[9] Ballerini G, Bardi U, Bignucolo R and Ceraolo G 2005 About some corrosion mechanisms of AZ91D magnesium alloy. *Corr. Sci.* 47: 2173–2184

[10] Song Y, Shan D, Chen R and Han En-Hou 2010 Effect of second phases on the corrosion behaviour of wrought Mg–Zn–Y–Zr alloy. *Corr. Sci.* 52: 1830–1837

[11] Ghasali E, Pakseresht A, Rahbari A, Eslami-Shahed H, Alizadeh M and Ebadzadeh T 2016 Mechanical properties and microstructure characterization of spark plasma and conventional sintering of Al-SiC-TiC composites. *J. Alloy Com.* 666: 366–371
[12] Ramesh Kannan C, Venkatesh R and Vivekanandan M 2022 Synthesis and Characterization of Mechanical Properties of AA8014 + Si3N4/ ZrO_2 Hybrid Composites by Stir Casting Process. *Journal of Advances in Materials Science and Engineering* **2022** Article ID 9150442, 11 pages
[13] Sivabalana R, Thangadurai K R and Lenin K 2021 Na_2CO_3 effect on high-strength lightweight ceramsite prepared from demagnesium boron mud and oil shale semi-coke. *J. Ceram. Process. Res.* 22: 605–614
[14] Kanakaraj A, Mohan R and Viswanathan R 2022 Parametric optimization of wear parameters on wear rate and coefficient of friction for hybrid (A356 + TiB_2 + ZrO_2) metal matrix composites. *J. Ceram. Process. Res.* 23: 268–277
[15] Baslayici, Serkan, Mehmet Bugdayci and MahmutErcanAcma 2021 Corrosion behaviour of hydroxyapatite-coated AZ31 and AZ91 Mg alloys by electrostatic spray coating. *J. Ceram. Process. Res*. 22: 98–105
[16] Satishkumar P and Natarajan N 2022 Investigation of mechanical properties and abrasive assisted electrochemical machining parameters on Al6061-10% TiB_2-3% Gr hybrid ceramic composite. *J. Ceram. Process. Res.* 23: 383–390
[17] Vinothkumar S and Senthilkumar P 2022 Experimental investigation and parametric optimization of stir casting process parameters for aluminium metal matrix composite. *J. Ceram. Process. Res.* 23: 546–552
[18] Sahin Y 2003 Preparation and some properties of SiC particle reinforced aluminium alloy composites. *Mater. Des.* 24: 671–679
[19] Zaid B, Saidi B, Benzaid A and Hadji S 2008 Effects of pH and chloride concentration on pitting corrosion of AA6061 aluminium alloy. *Corr. Sci.* 50: 1841–1847
[20] Umanath K, Palanikumar K and Selvamani S T 2013 Analysis of dry sliding wear behaviour of Al6061/SiC/Al_2O_3 hybrid metal matrix composites. *Compo: Part B*. **53** 159–168
[21] Venkatesh R, Manivannan S, Sakthivel P, Vijayan V and Jidesh S 2021 The Investigation on Newly Developed of Hydrophobic Coating on Cast AZ91D Magnesium Alloy Under 3.5 wt% NaCl Solutions. *J. Inorg. Organomet. Polym. Mater.* 32: 1246–1258
[22] Wang L, Zhang B P and Shinohara T 2010 Corrosion behaviour of AZ91 magnesium alloy in dilute NaCl solutions. *Mat. Des.* 31: 857–863
[23] Venkatesh R, Sakthivel P, Vivekanandan M, Ramesh Kannan C, Phani Krishna J, Dhanabalan S, Thirugnanasambandham T and Manaye Majora 2023 Synthesis and Thermal Adsorption Characteristics of Silver-Based Hybrid Nanocomposites for Automotive Friction Material Application. *Adsorp Sci Technol.* 1003492. https://doi.org/10.1155/2023/1003492
[24] Kanakaraj A, Mohan R and Viswanathan R 2022 Parametric optimization of wear parameters on wear rate and coefficient of friction for hybrid (A356 +TiB_2+ ZrO_2) metal matrix composites. *Int. J. Ceram. Process. Res.* 23: 268–277
[25] Umar Mohamed J, Palaniappan P L K, Maran P and Pandiyarajan R 2021 Influences of ZrO_2 and B_4C reinforcement on metallurgical, mechanical, and tribological properties of AA6082 hybrid composite materials. *J. Ceram. Process. Res.* 22: 306–316
[26] Kumar S, Vasumathi M, Begum R S, Luminitha S M, Vlase S and Pruncu C I 2012 Influence of B_4C and industrial waste fly ash reinforcement particles on the microstructural characteristics and mechanical behaviour of aluminium (Al–Mg–Si-T6) hybrid metal matrix composite. *J. Manuf. Proc.* 58: 668–676
[27] Velavan K, Palanikumar K, Natarajan E and Lim W H 2021 Implications on the influence of mica on the mechanical properties of cast hybrid (Al+ 10% B_4C+ Mica) metal matrix composite. *J. Mat. Res. Technol.* 10: 99–109
[28] Srinivasan A, Prabu R, Ramesh S and Viswanathan R 2022 Minimization of delamination, surface roughness and thrust force in drilling of Al_2O_3 ceramic particle filled CFRP composites. *Int. J. Ceram. Process. Res.* 23: 783–793
[29] Kumar J, Singh D, Kalsi N S, Sharma S, Pruncu C I and Pimenov D J 2020 Comparative study on the mechanical, tribological, morphological and structural properties of vortex casting processed, Al–SiC–Cr hybrid metal matrix composites for high strength wear-resistant applications: Fabrication and characterizations. *J. Mat. Res. Technol.* 9: 13607–13615
[30] Shin C S and Huang J C 2010 Effect of temper, specimen orientation and test temperature on the tensile and fatigue properties of SiC particles reinforced PM 6061 Al alloy. *Int. J. Fatig.* 32: 1573–1581
[31] Liu L, Wang Y, Muthuramalingam T and Anbuchezhiyan G 2019 Effect of B4C and MOS2 reinforcement on microstructure and wear properties of aluminium hybrid composite for automotive applications. *Compo. Part B: Eng.* 176: 107329
[32] Wang L, Shinohara T and Zhang Bio Ping 2009 Corrosion Behavior of AZ31 Magnesium Alloy in Dilute Sodium Chloride Solutions. *Zhang. Zairyo-to-Kankyo* 58: 105–110
[33] Lim T S, Ryu H S and Hong S H 2012 Electrochemical corrosion properties of CeO_2-containing coatings on AZ31 magnesium alloys prepared by plasma electrolytic oxidation. *Corr. Sci.* 62: 104–111
[34] Ahamad N, Mohammad A, Sadasivuni K K and Gupta P 2020 Phase, microstructure and tensile strength of Al–Al_2O_3–C hybrid metal matrix composites. *Procee. Instit. Mech Eng. Part C: J. Mech. Eng. Sci.* 234: 2681–2693
[35] Somasundaram M and Narendra Kumar U 2022 Electrochemical corrosion behaviour of stir cast and heat-treated EV31A magnesium alloy in different electrolytic mediums. *J. Appl. Electroche.* 53: 585–595
[36] Song J, She J, Chen D and Pan F 2020 Latest research advances on magnesium and magnesium alloys worldwide. *J. Magne. Alloy.* 8: 1–41
[37] Song S, Ma A, Jiang J, Lin P, Yang D and Fan J 2012 Corrosion behaviour of equal-channel-angular-pressed pure magnesium in NaCl aqueous solution. *Corr. Sci.* 52: 481–490
[38] Xie Q, Ma A, Jiang J, Liu H, Cheng Z and Gu, 2021 Tailoring the corrosion behaviour and mechanism of AZ31 magnesium alloys by different Ca contents for marine application. *Corr. Sci.* 192: 109842
[39] Atrens Andrej, Shi Zhiming, Mehreena Syeda, Johnston Sean, Song Guang-Ling, Chencand Xianhua and Fusheng Pan D 2020 Review of Mg alloy corrosion rates. *J. Magne and Alloy.* 8: 989–998